Nanoscale

PAPER

View Article Online
View Journal | View Issue

Cite this: *Nanoscale*, 2015, **7**, 15962

Thermoelectric properties of single-layered SnSe sheet†

Fancy Qian Wang,[a,b] Shunhong Zhang,[a,b] Jiabing Yu[c] and Qian Wang*[a,b]

Received 10th June 2015,
Accepted 21st August 2015

DOI: 10.1039/c5nr03813h

www.rsc.org/nanoscale

Motivated by the recent study of inspiring thermoelectric properties in bulk SnSe [Zhao *et al.*, *Nature*, 2014, **508**, 373] and the experimental synthesis of SnSe sheets [Chen *et al.*, *J. Am. Chem. Soc.*, 2013, **135**, 1213], we have carried out systematic calculations for a single-layered SnSe sheet focusing on its stability, electronic structure and thermoelectric properties by using density functional theory combined with Boltzmann transport theory. We have found that the sheet is dynamically and thermally stable with a band gap of 1.28 eV, and the figure of merit (*ZT*) reaches 3.27 (2.76) along the armchair (zigzag) direction with optimal n-type carrier concentration, which is enhanced nearly 7 times compared to its bulk counterpart at 700 K due to quantum confinement effect. Furthermore, we designed four types of thermoelectric couples by assembling single-layered SnSe sheets with different transport directions and doping types, and found that their efficiencies are all above 13%, which are higher than those of thermoelectric couples made of commercial bulk Bi_2Te_3 (7%–8%), suggesting the great potential of single-layered SnSe sheets for heat-electricity conversion.

Introduction

The performance of thermoelectric materials is typically quantified by the dimensionless figure of merit defined as $ZT = (S^2\sigma/\kappa)T$, where T, S, σ, and κ are the working temperature (in Kelvin), Seebeck coefficient, electrical conductivity, and thermal conductivity, respectively. The thermal conductivity κ is composed of both electronic (κ_e) and lattice (κ_l) contributions, *viz.* $\kappa = \kappa_e + \kappa_l$. However, the correlation and coupling among these physical parameters make it extremely difficult to improve the *ZT* value up to 3, which is the common research target for thermoelectric communities and considered to be essential for commercial utilization.[1] For instance, in the power factor $S^2\sigma$, the effect of the carrier concentration on the Seebeck coefficient and electrical conductivity is opposite: the reduction of the carrier concentration increases the Seebeck coefficient, but meanwhile results in lower electrical conductivity, and *vice versa*. Several approaches have been proposed to enhance the *ZT* value of bulk materials, such as modifying the band structure by doping heteroatoms[2] or distorting the lattice[3] to enhance the Seebeck coefficient; alloying[4] or introducing layered structures[5] to reduce lattice thermal conductivity. Nevertheless, the methods referred above all have limitations such as "alloying limits",[6] thus slow progress has been made in increasing the *ZT* value.

Another effective way to improve *ZT* is nanostructuring. Initially the investigations on 2D nanostructured thermoelectric materials were inspired by the prediction made by Hicks and Dresselhaus[7,8] in 1993 that the quantum confinement effect of electronic carriers in low-dimensional materials can dramatically enhance the power factor over that of their bulk counterparts. For example, it was demonstrated that nanostructuring of bulk Bi_2Te_3 can improve the *ZT* value thirteenfold. Such enhancement could be attributed to the sharp peaks in the electronic density of states (DOS) near the Fermi energy which improve electrical conductivity and impose asymmetry between holes and electrons transport, thus leading to a large Seebeck coefficient. Since then intensive attention has been paid to nanostructured materials and great progress has been made over the past two decades for many systems including Bi_2Te_3/Sb_2Te_3,[9] PbTe/Ag_2Te,[10] and silicon nanowires.[11]

Here we focus on SnSe, a typical metal chalcogenide with a layered structure and a narrow band gap. Recently, ultralow thermal conductivity (<0.25 W m^{-1} K^{-1}) and high thermoelectric figure of merit (2.6 ± 0.3) at T = 935 K along the specific axis in bulk SnSe crystals have been reported by Zhao *et al.*,[12] showing that high thermoelectric performance can be realized in a simple compound with advantages of chemical stability, non-toxicity and earth abundance. Meanwhile, considerable

[a]*Center for Applied Physics and Technology, College of Engineering, Peking University, Beijing 100871, China. E-mail: qianwang2@pku.edu.cn*
[b]*Key Laboratory of High Energy Density Physics Simulation, and IFSA Collaborative Innovation Center, Ministry of Education, Beijing 100871, China*
[c]*Department of Materials Science and Engineering, College of Engineering, Peking University, Beijing 100871, China*
†Electronic supplementary information (ESI) available. See DOI: 10.1039/c5nr03813h

attention has been paid to the thermoelectric properties of polycrystalline SnSe.[13–20] In addition to bulk phases, nanostructured SnSe has also been intensively studied and bears broad applications in the fields of solar cells,[21] supercapacitors,[22] anodes for lithium-ion batteries,[23] and infrared optoelectronic devices.[24] For instance, a single-crystalline SnSe nanosheet with four-atomic thickness was synthesized for the first time in 2013,[25] a phase-controlled method to synthesize SnSe nanosheets was proposed,[22] thin films of $Cd_xSn_{1-x}Se$ with the compositions controlled by electrodeposition techniques were successfully synthesized.[26] Since the thermoelectric performance of materials can be enhanced by reducing dimensionality, we are curious about whether a single-layered SnSe sheet can display a high *ZT* value. Theoretically, it has been found that a single-layered SnSe sheet exhibits low formation energy (about 200 meV per atom)[27] due to the interlayer weak van der Waals force and strong covalent bonds within each layer. So it could be easy to extract a single-layered SnSe sheet from the layered bulk material without any substrates. Although the structural stability of a single-layered SnSe sheet has been discussed,[28] its thermoelectric performance has not yet been studied. Therefore it is highly desirable to explore the thermal stability, electronic and phononic properties, and thermoelectric performance of single-layered SnSe sheets.

Based on first-principles calculations combined with Boltzmann transport theory, we have systematically studied the single-layered SnSe sheet focusing on its dynamical and thermal stabilities, Seebeck coefficient, electrical conductivity, thermal conductivity, and figure of merit (*ZT*). At 700 K, the peak *ZT* value of the single-layered SnSe sheet reaches 3.27, enhanced nearly 7 times compared to its bulk phase at the same temperature.

In practical applications, thermoelectric materials are widely used for heat-electricity conversion or refrigeration.[29] To this end, semiconducting thermoelectric materials of different doping types are usually assembled into devices such as thermoelectric couples or coolers. We further demonstrate that a single-layered SnSe sheet with different doping types can be assembled into thermoelectric devices, and both the zigzag and armchair directions are suitable for the transport to achieve high efficiency.

Computational methods

We start by relaxing the atomic structure and calculating an electronic structure of the single-layered SnSe sheet using the density functional theory (DFT) and projector augmented wave (PAW) method as implemented in the Vienna Ab initio Simulation Package (VASP).[30] Perdew–Burke–Ernzerhof (PBE) functional within generalized gradient approximation (GGA)[31] is used to treat the electronic exchange–correlation interaction. The accurate band gap is also calculated using the Heyd–Scuseria–Ernzerhof (HSE06)[32] functional for better assessment of the electrical properties. The kinetic energy cutoff of wave functions is set to be 400 eV, and a Monkhorst–Pack *k*-mesh of $15 \times 15 \times 1$ is used to sample the Brillouin Zone (BZ) for integrations in reciprocal space. A large vacuum space of at least 16.33 Å is used to hinder the interactions between periodic layers arising from the employed periodic boundary conditions. All atomic positions are fully optimized without any symmetry constraint until the maximal Hellmann–Feynman forces are smaller than 10^{-2} eV Å^{-1}.

After investigating the basic structural stability and electronic properties of the single-layered SnSe sheet, we studied its thermoelectric properties including electronic transport properties by solving the semi-classical Boltzmann transport equation within the constant relaxation time approximation as implemented in the BoltzTraP[33] program, as well as lattice thermal conductivity evaluated from self-consistently calculated phonon lifetimes as implemented in the ShengBTE[34] code. Such a combined method has been applied to calculate the thermoelectric properties of many materials and yields satisfactory accuracy and predictive power.[35,36]

We computed the second-order harmonic interatomic force constants (IFCs) using $5 \times 5 \times 1$ supercells generated by using the Phonopy[37] package, and third-order anharmonic IFCs[38] using $4 \times 4 \times 1$ supercells created by using the ShengBTE[34] code focusing on the phonon–phonon Umklapp process. All the required atomic forces were obtained from DFT calculations performed by using VASP. Considering both symmetry and calculation accuracy some important parameters including an appropriate cutoff radius of 6.5 Å (up to 21st nearest neighbors), a scale broad[39] of 1.0 and a *k*-mesh of $30 \times 30 \times 1$ are selected. Details of the convergence test can be found in the ESI.† In addition, considering the long-range Coulomb interactions, the dielectric parameters of the system including a set of Born effective charge and the dielectric tensor in the infinite-frequency limit are involved.

Results and discussion

Bulk SnSe has two structurally similar phases, namely, the low temperature *Pnma* phase and the high temperature *Cmcm* phase, and both of them consist of weakly bound identical layers. Therefore, we computationally peel a single layer from the low temperature *Pnma* bulk structure and fully relax it. As shown in Fig. 1, the optimized configuration of the single-layered SnSe sheet possesses $Pm2_1n$ symmetry (layer group no. 32) with an orthogonal lattice, which is lower than that of its bulk counterpart due to the lack of inversion symmetry. The single-layered SnSe has a highly puckered honeycomb structure, similar to that of the recently synthesized monolayer black phosphorus (phosphorene).[40] We thereby denote the zigzag and armchair directions (Fig. 1a) in the nanosheet following previous studies on phosphorene. The obtained lattice constants are quite close, with the values of 4.307 Å and 4.362 Å respectively along the zigzag and armchair directions, which are in reasonable agreement with the previous literature.[28]

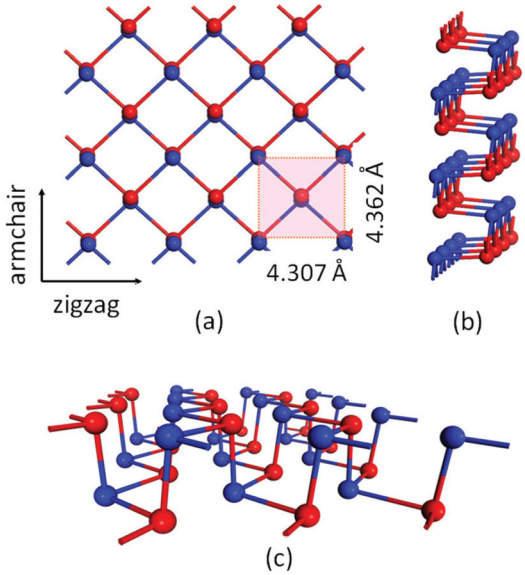

Fig. 1 (a) Top view and (b) side view of optimized atomic configuration of the single-layered SnSe sheet. The perspective view is given in (c). The shadow marked in yellow dashed lines denotes a unit cell containing 4 atoms: blue and red balls represent Sn and Se atoms, respectively. The zigzag and armchair directions are indicated in (a).

To confirm the dynamical stability of the single-layered SnSe, phonon dispersion is calculated in the framework of the density functional perturbation theory.[41] The results are plotted in Fig. 2a. The longitudinal acoustic (LA) branch and the transversal acoustic (TA) branch have linear dispersions as the wave vector approaches Γ point, whereas the out-of-plane ZA branch exhibits a parabolic dispersion due to the rapid decay of transversal forces.[42] No appreciable imaginary modes are found in the first Brillouin zone, suggesting that the single-layered SnSe is dynamically stable.

To further study its thermal stability at finite-temperature, we performed *ab initio* molecular dynamics (MD) simulations at different temperatures (from 300 K to 900 K) using the canonical (NVT) ensemble. A 4 × 4 × 1 supercell is constructed to simulate the 2D sheet for minimizing the constraint induced by periodicity. We found that the geometry of the single-layered structure remains nearly intact and the total energies remain almost invariant after heating for more than 10 picoseconds at typical temperatures. Therefore, the single-layered SnSe sheet is thermally stable in a wide temperature range from 300 K to 900 K. However, the layered structure starts decomposing when heated to 1000 K, and the total energy no longer remains invariant during simulations. Therefore, we conclude that the single-layered SnSe sheet at least can sustain temperature as high as 900 K. The simulated results at 700 K are given in Fig. 2b, and all the others are provided in Fig. S3 in the ESI.† We also looked at the bond length variance during the MD simulations. The details can be found in Table S1 in the ESI.† It is well known that the bulk SnSe undergoes a phase transition from a lower symmetry (space group *Pnma* #62) phase to a higher symmetry (space group *Cmcm* #63) phase at around 750–800 K. We assumed that the single-layered SnSe sheet may also experience a similar phase transition to other possible allotropes upon heating like bulk SnSe. However, the phase transition is beyond the scope of this study. Thus we only concentrated on the medium–high temperature range (300–700 K), and chose 700 K as a typical temperature to perform the thermoelectric calculations.

Next we calculate the electronic band structure of the single-layered SnSe sheet, which is closely related to the Seebeck coefficient and electrical conductivity. The calculated band structure of the single-layered SnSe sheet and its corresponding total DOS are plotted in Fig. 3. At the GGA-PBE level, the single-layered SnSe is predicted to be a quasi-direct-band-gap semiconductor with a band gap of 0.914 eV. The band gap size is much larger than that of the bulk SnSe (0.39 eV for *Pnma* phase and 0.61 eV for *Cmcm* phase, calculated using PBE functional[12]) due to the weak interaction between the layers. The valance band maximum (VBM) is located on the Γ–Y path, while there exists two energetically nearly degenerate conduc-

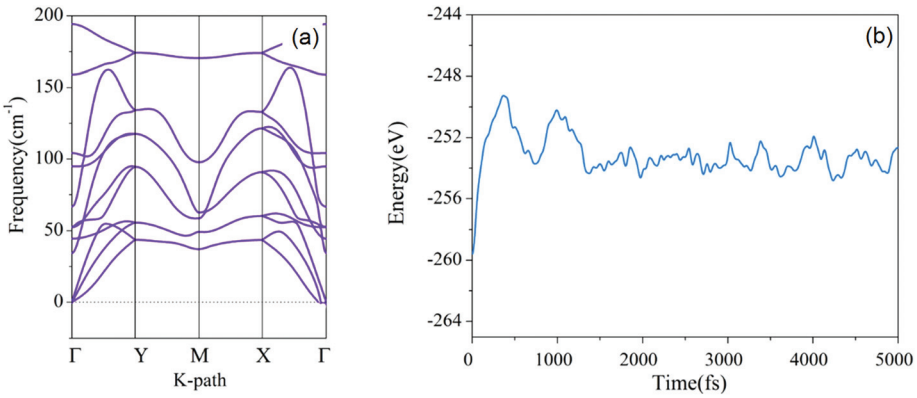

Fig. 2 (a) Phonon dispersion band structure along the high symmetric *k*-point path in the first Brillouin zone. The high symmetry *k* points are: Γ (0, 0, 0), Y (0, 1/2, 0), M (1/2, 1/2, 0), and X (1/2, 0, 0). (b) Energy fluctuation with respect to time in *ab initio* molecular dynamics simulations at 700 K.

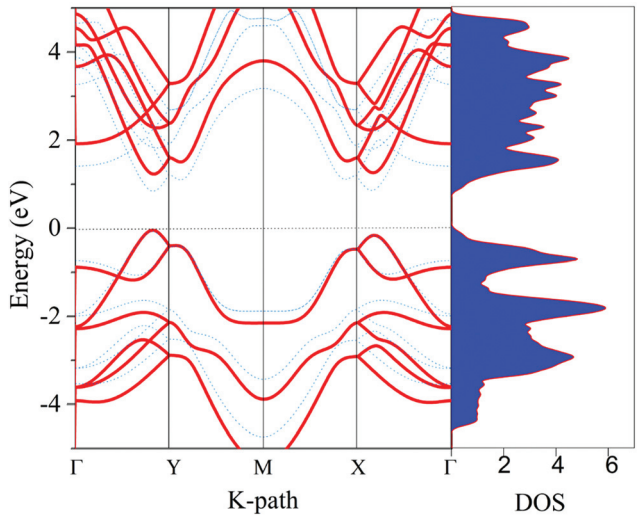

Fig. 3 Electronic band structure of the single-layered SnSe based on PBE (blue dashed line) and HSE06 (red solid line) functionals and the corresponding density of states (DOS). The Fermi energy level is shift to 0 eV.

tion band minimums (CBMs), one is on the Γ–Y path, and the other is on the Γ–X path. Considering the underestimation of band gaps in conventional DFT calculations, we repeat the above calculation using the HSE06 functional with 25% Fock exchange to predict a more accurate band gap, which is crucial to thermoelectric properties especially at elevated temperatures.[43] Although the band dispersion obtained by using the HSE06 functional is similar to that obtained by using the PBE functional, the band gap increases to 1.28 eV. Such band gap size is significantly larger than previously studied narrow gap metal chalcogenides (like Bi_2Te_3) and can effectively overcome the high temperature bipolar conduction problem which may degrade the thermoelectric performance.[44] We can also see from the band structure that both the valence and conduction bands have a typical characteristic named "pudding mold" proposed by Kuroki and Arita,[45] namely, a peculiar shape of the band contains a flat portion with some corrugations at the top (bottom) while sharply bends into a highly dispersive portion below (above) resulting in multiple Fermi surfaces, which is in favor of a high Seebeck coefficient and electrical conductivity.

To examine the ability of producing voltage from the temperature difference in a circuit, the Seebeck coefficient of the single-layered SnSe as a function of chemical potential (μ) at different temperatures is calculated by solving the Boltzmann Transport Equation (BTE) using the BoltzTraP code and plotted in Fig. 4a and b. The coefficient varies dramatically with chemical potential, indicating that an optimal carrier concentration is beneficial to achieve efficient thermoelectric performance. The Seebeck coefficient degrades rapidly with elevated temperature due to a bipolar conduction effect or the excitation of carriers with both positive and negative charges suggesting an increasing inverse Hall coefficient.[44] The peak value of the Seebeck coefficient of the n-type single-layered SnSe at room temperature along the zigzag (armchair) direction is 2150 μV K^{-1} (2080 μV K^{-1}), while that of the p-type single-layer is 2160 μV K^{-1} (2200 μV K^{-1}), which are enhanced nearly four times as compared with that of the bulk SnSe.

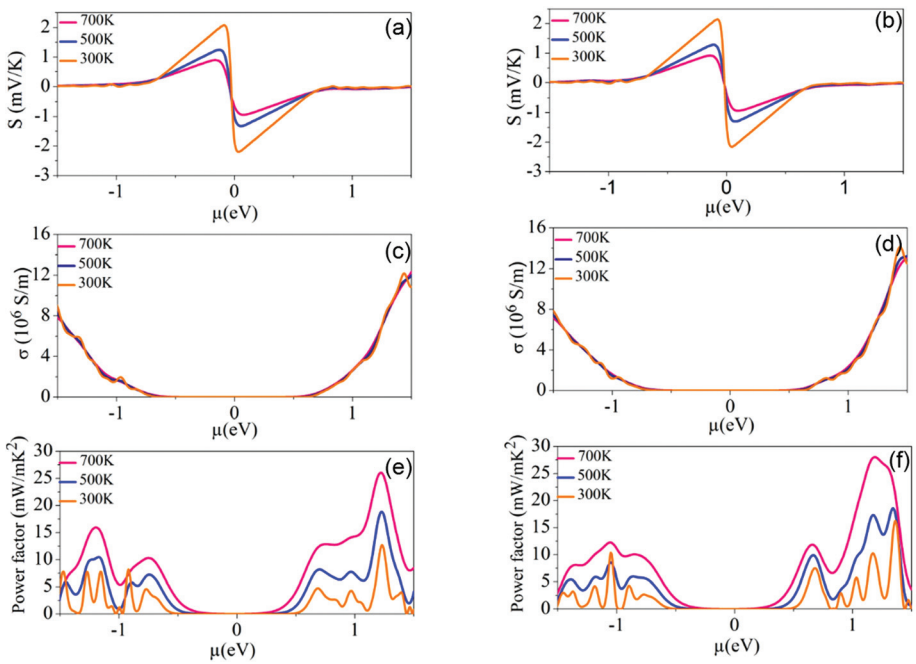

Fig. 4 Calculated electronic transport parameters as a function of chemical potential at different temperatures along the zigzag (left column) and armchair (right column) directions: (a) and (b) Seebeck coefficient, (c) and (d) electrical conductivity, (e) and (f) power factor.

Even at high temperature (700 K), the peak value in the zigzag (armchair) direction also reaches 921 μV K^{-1} (898 μV K^{-1}) for the p-type doping, and 938 μV K^{-1} (945 μV K^{-1}) for the n-type doping, which are about three-fold larger than that of the bulk SnSe. This remarkable enhancement can be ascribed to the quantum confinement effect which induces sharp DOS peaks near the Fermi energy.

Within the semi-classical Boltzmann transport theory, the electrical conductivity σ can be estimated only if the electron relaxation time τ is given. Actually, the BoltzTraP[33] code only outputs a ratio σ/τ in form of nine individual components of the conductivity tensor. The "in-plane" electrical conductivity from the experiment along the zigzag and armchair directions at room temperature was reported to be nearly 10 S cm^{-1}.[29] Using the average value of the diagonal components of σ/τ at the experiment conductivity, we determine that the relaxation time is $\tau = 2.93 \times 10^{-14}$ s, which is within the reasonable range.[46] Such method has been implemented to estimate the relaxation time in many other materials.[35,47] The electrical conductivity is acquired when we insert the relaxation time into each component of σ/τ. The calculated electrical conductivity as a function of chemical potential μ at different temperatures is plotted in Fig. 4c and d. Unlike the Seebeck coefficient the electric conductivity is less sensitive to temperature. Quite large electrical conductivity is achieved with increasing μ. However, S always reaches a peak value near the Fermi energy (smaller μ), so the better trade-off between the Seebeck coefficient and electrical conductivity resulting in high power factor is critical for good thermoelectric performance. This can be easily explained using the DOS: because electrons and holes have opposite signs in the Seebeck coefficient, actually the absolute Seebeck coefficient which means average energy transported by the carriers is what we measured in the experiment or calculated in theory. Considering only the carriers near the Fermi energy level have contributions to the conduction process at finite temperature, when the Fermi level is close to the band edge through appropriate doping, the DOS becomes asymmetric with respect to the Fermi level, namely, different numbers of states are available for carrier transport on both sides of the Fermi level, thus resulting in a large absolute Seebeck coefficient. At the same time, the high DOS near Fermi energy provides large enough electrical conductivity. Consequently, the power factor ($S^2\sigma$) of the single-layered SnSe shown in Fig. 4e and f is larger than that of usual thermoelectric materials.

We next study the thermal conductivity of the single-layered SnSe. In non-degenerate semiconductors, both electrons and phonons contribute substantially to the total thermal conductivity. This is different from the situation in metals or degenerate semiconductors where electronic contribution to thermal conductivity is negligible. The electrical conductivity σ is tied to electrical thermal conductivity κ_e through an important relationship known as Wiedemann–Franz law,[48] namely, $\kappa_e = L\sigma T$, where L is the Lorenz number. In the special case of non-degenerate semiconductors limited by phonon scattering,[45] L is approximately 1.5×10^{-8} W Ω K^{-2}. Consequently, the κ_e–T curves (Fig. 5a) exhibit similar trends to σ. The intrinsic lattice thermal conductivity of the single-layered SnSe sheet at different temperatures is estimated using the ShengBTE[34] code based on the phonon Boltzmann transport equation. The temperature dependence of axial lattice thermal conductivity is shown in Fig. 5c. The fitted line well satisfies the relationship $\kappa_l \propto \frac{1}{T}$ as presented in Fig. 5d, indicating that anharmonic phonon–phonon interactions are dominant in the phonon scattering mechanism,[49] the detailed discussion can be found in the ESI.† The values along the zigzag (2.5 W m^{-1} K^{-1}) and armchair directions (2.02 W m^{-1} K^{-1}) at room temperature are not only nearly isotropic but also lower than those of many synthetic two dimensional (2D) nanostructures, such as monolayered MoS_2 (26.2 W m^{-1} K^{-1}),[50] graphene (~2000 W m^{-1} K^{-1}),[51] and phosphorene (83.5 W m^{-1} K^{-1}, 24.3 W m^{-1} K^{-1}),[52] especially comparable to those state-of-the-art thermoelectric materials such as Bi_2Te_3 (1.5 W m^{-1} K^{-1}) and PbTe (2.01 W m^{-1} K^{-1}).[53] The low intrinsic thermal conductivity is a combined consequence of the heavy constituent elements and the low atomic coordination, which led to low frequency optical branches overlapping with the acoustic branches seen clearly from the phonon spectrum. So we believe that the optical branches carry a similar amount of heat as acoustic modes. Actually, at room temperature, the contributions to thermal conductivity of three acoustic branches (ZA, TA, LA) along the zigzag direction are respectively 30%, 22%, 15.8%, while along the armchair direction these values are 32.8%, 18.4%, 15.6%. On the other hand, the quasi-acoustic branches have commensurate total contributions: 32.2% along the zigzag direction and 33.2% along the armchair direction, which resembles the case of bulk WS_2.[35] We additionally found that the single-layered SnSe sheet has a character of soft modes which means low Debye temperature and small sound velocities. These soft modes are the symbol of weak interatomic bonds related to strong anharmonicity leading to lower thermal conductivity. For example, along the armchair direction, the Debye temperatures of the two linear acoustic branches (TA, LA) are 137 and 151 K, respectively, and the corresponding sound velocities are 1906 and 3545 m s^{-1}, which are much smaller than many other 2D materials. To better understand the origin of the low thermal conductivity, the mode Grüneisen parameter (γ) of the acoustic modes is calculated to quantify the extent of anharmonicity. The results are presented in Fig. S4 in the ESI.† The average Grüneisen parameter along the zigzag and armchair directions is 1.65 and 2.03, respectively, which is comparable with PbTe (1.96)[53] and $AgSbTe_2$ (2.05).[54] However, it should be mentioned that the calculated thermal conductivity of the single-layered SnSe sheet is slightly larger than that of the bulk SnSe,[12] which possibly originates from the following reasons: (1) the calculated value usually exceeds the experimentally measured value because the latter contains other scattering sources such as boundary, defect, and impurity; (2) the single-layered SnSe sheet loses the distorted $SnSe_7$ polyhedra structure while maintaining the zigzag accordion-like geometry of slabs, which weakens the anharmonicity of the single-layered

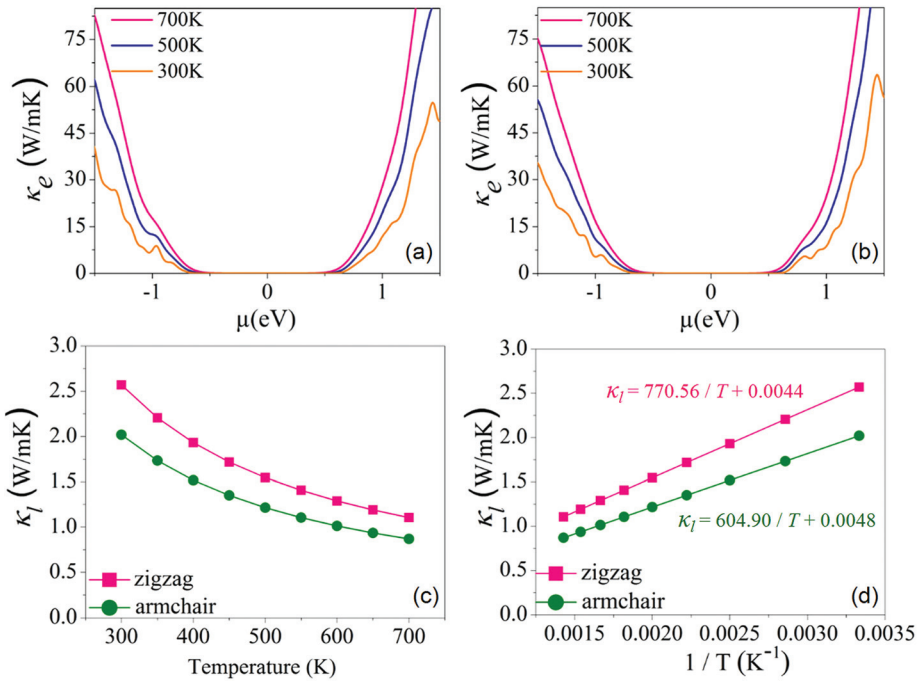

Fig. 5 Electronic contribution to the thermal conductivity of the single-layered SnSe as a function of chemical potential at different temperatures along (a) the zigzag direction (b) the armchair direction. (c) Lattice thermal conductivity of the single-layered SnSe as a function of temperature along the two directions. (d) The fitted relationship $\kappa_l \propto \frac{1}{T}$.

SnSe sheet because both the two parts play vital roles in decreasing κ_l according to Zhao *et al.*[12] A similar phenomenon has been reported in phosphorene.[52]

With all the transport coefficients available, the *ZT* value of the single-layered SnSe sheet as a function of chemical potential at different temperatures is obtained as shown in Fig. 6. We can see that the *ZT* values increase with elevated temperatures along both the zigzag and armchair directions. At 700 K, the *ZT* values reach the maximum 2.47 at chemical potential $\mu = -0.62$ eV and 2.76 at chemical potential $\mu = 0.575$ eV along the zigzag direction. Meanwhile, the maximal *ZT* values of 2.51 and 3.27 along the armchair direction are observed at $\mu = -0.63$ eV and $\mu = 0.54$ eV, respectively. The *ZT* values calculated in this work approach commercial demands, indicating great potential of the single-layered SnSe sheet as a 2D high performance thermoelectric material.

Although the calculated *ZT* values are intriguing, a discrepancy may exist between the DFT calculations and experiments. It is well known that DFT calculations usually overestimate the *ZT* values as compared to the experimental

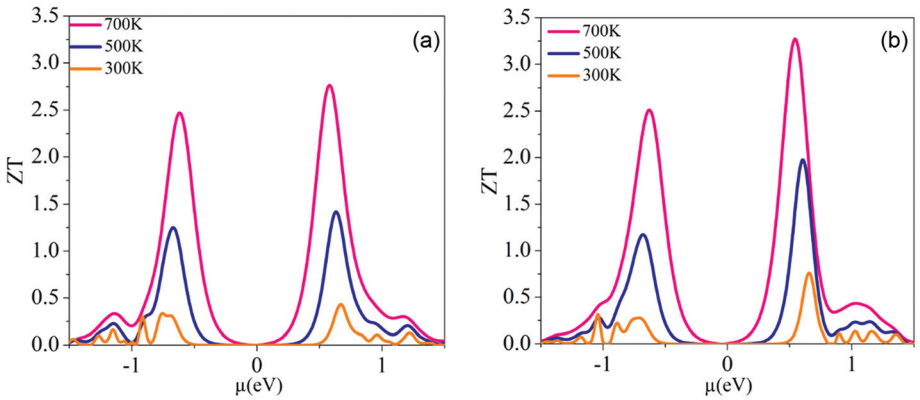

Fig. 6 Figure of merit (*ZT*) of the single-layered SnSe as a function of the chemical potential at different temperatures along (a) the zigzag and (b) the armchair direction.

results. In our calculations, the possible reasons to cause such discrepancy are: the constant relaxation time approximation adopted when calculating the electrical conductivity and the neglect of some scattering processes when calculating the thermal conductivity. More precisely: the relaxation time is direction-dependent and varies with temperature and carrier concentration in real systems. Moreover, the same relaxation time is used for electrons and holes when considering a similar carrier scattering process. This simplest approximation is effective and reasonable to some extent, while also limits the accuracy of prediction inevitably. Considering the accessibility of experimental data, we used the relaxation time estimated at low temperature. Indeed, with the temperature elevated, the relaxation time might become shorter as the carrier concentration increases. In this sense the electrical conductivity may be overestimated, while for the thermal conductivity, only the three-phonon scattering rates and isotopic impurity scattering rates are considered during our calculations. Actually, there are many other scattering processes in real systems such as point defect scattering, grain boundary scattering, and dislocation scattering that also have some influence on thermal conductivity, most likely reducing the thermal conductivity. In this sense, our calculated thermal conductivity of the single-layered SnSe may have been overestimated. Therefore, the errors introduced from the overestimation of electrical and thermal conductivities may cancel out to some extent. Consequently, our calculated ZT values would be in reasonable agreement with the experimental data.

So far, we have theoretically predicted the enhanced thermoelectric power of the single-layered SnSe sheet and elucidated its microscopic origin by studying its vibrational and electronic properties. We then discuss its implementation in devices. Generally, thermoelectrics are used in two ways: the Seebeck effect which directly converses heat into electricity can be applied in thermoelectric couples for power generation; while the Peltier effect which adsorbs heat at the electrified junctions can be used for refrigeration. Here, we concentrate on the performance of the single-layered SnSe sheet in power generation, namely, heat-electricity conversion.

Although the ZT value is widely used to evaluate the preliminary thermoelectric properties of a material, in devices it is necessary to directly access its performance by considering the energy conversion efficiency. The efficiency of a thermoelectric material (called a thermoelectric segment when incorporated into a thermoelectric device) is defined as $\eta = \eta_r\eta_c$, where $\eta_c = (T_h - T_c)/T_h$ (where T_h and T_c represent the temperature of the heat resource and cold side) is the Carnot efficiency, and η_r is the reduced efficiency.[55] Two factors can influence the total energy conversion efficiency. The first is the temperature difference ($\Delta T = T_h - T_c$) which determines the upper-limit efficiency of a Carnot engine. The upper limit of the ΔT is limited by thermal stability of the thermoelectric. The second is the relative current density $u = J/\kappa\nabla T$ where J is the electric current density. It has been demonstrated that η_r reaches the maximum value only if u is equal to the compatibility factor, s, which is defined as $s = \frac{\sqrt{1+ZT}-1}{ST}$.[29,55] Considering the transport directions and doping types, there are four types of single-layered SnSe-based segments, namely, Zp, Zn, Ap, and An, where Z and A refer to the zigzag and armchair direction, n and p represent n-type and p-type doping, respectively. The calculated compatibility factors of the four thermoelectric segments are shown in Fig. 7a. It is encouraging that the compatibility factors are almost in the range of 3 to 5 V^{-1} over the whole operating temperature range (300 K–700 K), implying that these four thermoelectric materials are well matched with the above conditions. Furthermore, the s–T curve is fairly flat, manifesting that each thermoelectric material possesses the preferable self-compatibility, which provides a good chance to assemble single-layered SnSe sheets into a segmented thermoelectric couples is illustrated in Fig. 7b. In such a thermoelectric couple, the two segments are "electrically in series and thermally in parallel", hence the total efficiency will significantly decrease if the compatibility factors differ more than 2 times between different thermoelectric segments. It is noteworthy that the difference in compatibility factors between the doped SnSe sheets and other popular thermoelectric materials, such as p-type TAGS (s = 2.5–4), $CeFe_4Sb_{12}$ ($s \approx 3$),[56] n-type PbTe (s = 4–1.5), $CoSb_3$ ($s \approx 2$),[57] is within "the factor of 2", therefore single-layered SnSe sheets might be assembled with all of them to form a segmented device with high performance.

For simplicity, we consider here a thermoelectric couple composed of the two single layered SnSe segments with different doping types. Four combinations can be involved: ZpZn, ApAn, ZpAn, and ZnAp. The ideal dimensionless Z_cT of a thermoelectric couple assembled by the p- and n-type thermoelectric segments can be calculated through the expression $Z_cT = \frac{{S_c}^2T}{\kappa_c\rho_c} = \frac{(S_p - S_n)^2T}{(\kappa_p + \kappa_n)(\rho_p + \rho_n)}$.[22] The calculated Z_cTs for the four thermoelectric couples are presented in Fig. 7c.

The ideal maximum efficiency (η) characterizes the ability of thermoelectric couple conversion between electricity and heat directly. We evaluate four kinds of segmented thermoelectric couples using the simple equation[58]

$$\eta = \eta_c \frac{\sqrt{1+\overline{Z_cT}}-1}{\sqrt{1+\overline{Z_cT}}+T_c/T_h}$$

In our calculations T_c is set at 300 K and T_h varies from 300 K to 700 K. Here we assume that the relative current density is equal to the compatibility factor ($u = s$) in each stage. The results plotted in Fig. 7d indicate that the total efficiency η reaches 16.46% (ZnZp), 17.03% (AnAp), 15.04% (ZpAn), and 13.97% (ZnAp), respectively, when temperature difference is 400 K (T_h = 700 K). Such magnitudes are higher than previously reported efficiencies in thermoelectric couples made of commercial bulk Bi_2Te_3.[22]

At present, it is still challenging to implement 2D materials in real modules. However, single-layered material based devices have now become achievable[40,59,60] and such kinds of thermoelectric modules are possible in principle.

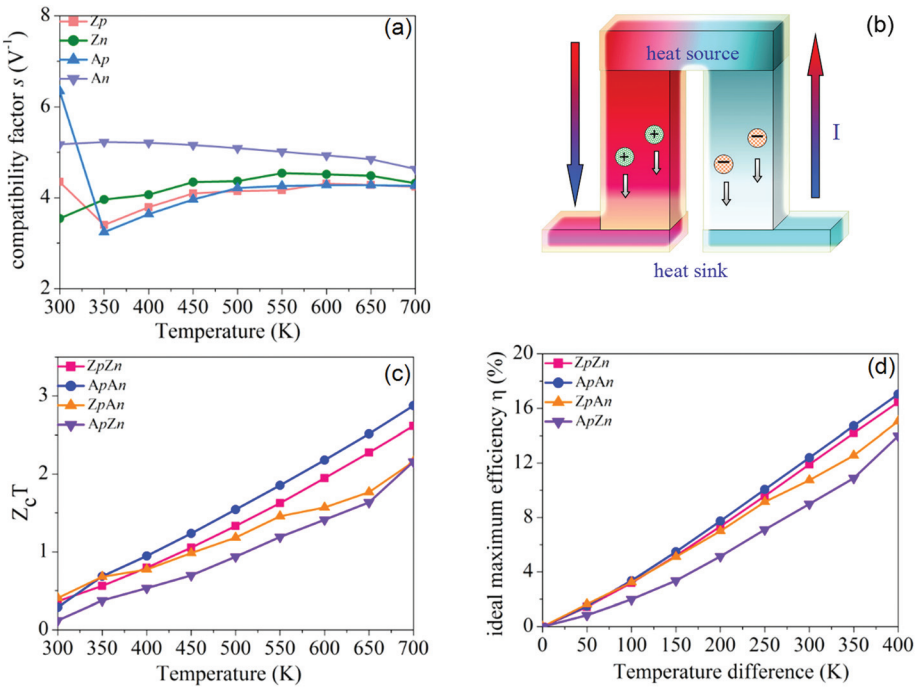

Fig. 7 (a) Compatibility factor s of four single-layered SnSe based thermoelectric segments. (b) Schematic illustration of a thermoelectric couple comprising a p-type (left) and an n-type (right) segment. (c) Z_cT of four types of thermoelectric couples: ZpZn, ApAn, ZpAn, and ZnAp; and (d) the corresponding ideal maximum efficiency.

Conclusions

We have used DFT combined with semi-classical BTE to assess the intrinsic thermoelectric capabilities of a single-layered SnSe sheet for the first time, and found that the power factor of the single-layered SnSe is significantly enhanced compared to the bulk SnSe due to strong quantum confinement effect. Meanwhile, the ultralow intrinsic thermal conductivity of 2.57 W m^{-1} K^{-1} (zigzag)/2.02 W m^{-1} K^{-1} (armchair) evaluated at room temperature is close to the typical thermal conductivity of good thermoelectric materials (κ < 2 W m^{-1} K^{-1}). The optimal direction is the armchair direction, which reveals the highest ZT value of 3.27 (at 700 K) when the system is n-type doped with an appropriate concentration, which is 7 times higher than that of the bulk SnSe at the same temperature. In addition, the four types of single-layered SnSe not only exhibit suitable compatibility factors with many other practical materials but also have self-compatibility, thus providing good opportunity to be assembled as effective thermoelectric couples. The ideal maximum efficiencies of the four thermoelectric couples are 16.46% (ZnZp), 17.03% (AnAp), 15.04% (ZpAn), and 13.97% (ZnAp) respectively under appropriate operating temperature, higher than the efficiency of commercially used bulk Bi_2Te_3. We demonstrated that the single-layered SnSe is a promising thermoelectric material that could be applied in nanoscale thermoelectric devices such as thermoelectric couples. We expect the advent of nanotechnology will facilitate the integration of nanostructured SnSe into thermoelectric devices for practical applications.

Acknowledgements

This work is partially supported by grants from the National Natural Science Foundation of China (NSFC-11174014, NSFC-21273012), the National Grand Fundamental Research 973 Program of China (Grant No. 2012CB921404), and the Doctoral Program of Higher Education of China (20130001110033).

References

1 C. J. Vineis, A. Shakouri, A. Majumdar and M. G. Kanatzidis, *Adv. Mater.*, 2010, **22**, 3970–3980.
2 W.-S. Liu, L.-D. Zhao, B.-P. Zhang, H.-L. Zhang and J.-F. Li, *Appl. Phys. Lett.*, 2008, **93**, 042109.
3 J. P. Heremans, V. Jovovic, E. S. Toberer, A. Saramat, K. Kurosaki, A. Charoenphakdee, S. Yamanaka and G. J. Snyder, *Science*, 2008, **321**, 554–557.
4 D. Rowe, V. Shukla and N. Savvides, *Nature*, 1981, **290**, 765–766.
5 K. Biswas, J. He, I. D. Blum, C.-I. Wu, T. P. Hogan, D. N. Seidman, V. P. Dravid and M. G. Kanatzidis, *Nature*, 2012, **489**, 414–418.
6 K. Koumoto, Y. Wang, R. Zhang, A. Kosuga and R. Funahashi, *Annu. Rev. Mater. Res.*, 2010, **40**, 363–394.
7 L. Hicks and M. Dresselhaus, *Phys. Rev. B: Condens. Matter*, 1993, **47**, 12727.
8 L. Hicks, T. Harman and M. Dresselhaus, *Appl. Phys. Lett.*, 1993, **63**, 3230–3232.

9 R. Venkatasubramanian, E. Siivola, T. Colpitts and B. O'quinn, *Nature*, 2001, **413**, 597–602.
10 J. J. Urban, D. V. Talapin, E. V. Shevchenko, C. R. Kagan and C. B. Murray, *Nat. Mater.*, 2007, **6**, 115–121.
11 A. I. Boukai, Y. Bunimovich, J. Tahir-Kheli, J.-K. Yu, W. A. Goddard Iii and J. R. Heath, *Nature*, 2008, **451**, 168–171.
12 L.-D. Zhao, S.-H. Lo, Y. Zhang, H. Sun, G. Tan, C. Uher, C. Wolverton, V. P. Dravid and M. G. Kanatzidis, *Nature*, 2014, **508**, 373–377.
13 S. Sassi, C. Candolfi, J.-B. Vaney, V. Ohorodniichuk, P. Masschelein, A. Dauscher and B. Lenoir, *Appl. Phys. Lett.*, 2014, **104**, 212105.
14 S. Sassi, C. Candolfi, J.-B. Vaney, V. Ohorodniichuk, P. Masschelein, A. Dauscher and B. Lenoir, *Mater. Today*, 2015, **2**, 690–698.
15 C.-L. Chen, H. Wang, Y.-Y. Chen, T. Day and G. J. Snyder, *J. Mater. Chem. A*, 2014, **2**, 11171–11176.
16 Y. Li, X. Shi, D. Ren, J. Chen and L. Chen, *Energies*, 2015, **8**, 6275–6285.
17 K. Kutorasinski, B. Wiendlocha, S. Kaprzyk and J. Tobola, *Phys. Rev. B: Condens. Matter*, 2015, **91**, 205201.
18 A. Hong, L. Li, H. Zhu, Z. Yan, J. Liu and Z. Ren, *J. Mater. Chem. A*, 2015, **3**, 13365.
19 R. Guo, X. Wang, Y. Kuang and B. Huang, 2015, arXiv preprint arXiv:1505.02601.
20 J. Carrete, N. Mingo and S. Curtarolo, *Appl. Phys. Lett.*, 2014, **105**, 101907.
21 M. A. Franzman, C. W. Schlenker, M. E. Thompson and R. L. Brutchey, *J. Am. Chem. Soc.*, 2010, **132**, 4060–4061.
22 C. Zhang, H. Yin, M. Han, Z. Dai, H. Pang, Y. Zheng, Y.-Q. Lan, J. Bao and J. Zhu, *ACS Nano*, 2014, **8**, 3761–3770.
23 M.-Z. Xue, J. Yao, S.-C. Cheng and Z.-W. Fu, *J. Electrochem. Soc.*, 2006, **153**, A270–A274.
24 T. Subba Rao and A. K. Chaudhuri, *Bull. Mater. Sci.*, 1996, **19**, 449–453.
25 L. Li, Z. Chen, Y. Hu, X. Wang, T. Zhang, W. Chen and Q. Wang, *J. Am. Chem. Soc.*, 2013, **135**, 1213–1216.
26 V. Dhanasekaran, J. Jung, K. K. Lee and T. Mahalingam, *Ionics*, 2014, 1–6.
27 A. K. Singh, K. Mathew, H. L. Zhuang and R. G. Hennig, *J. Phys. Chem. Lett.*, 2015, **6**, 1087–1098.
28 A. K. Singh and R. G. Hennig, *Appl. Phys. Lett.*, 2014, **105**, 042103.
29 G. J. Snyder, *Appl. Phys. Lett.*, 2004, **84**, 2436–2438.
30 G. Kresse and J. Furthmüller, *Phys. Rev. B: Condens. Matter*, 1996, **54**, 11169.
31 J. P. Perdew, K. Burke and M. Ernzerhof, *Phys. Rev. Lett.*, 1996, **77**, 3865.
32 J. Heyd and G. E. Scuseria, *J. Chem. Phys.*, 2004, **121**, 1187–1192.
33 G. K. Madsen and D. J. Singh, *Comput. Phys. Commun.*, 2006, **175**, 67–71.
34 W. Li, J. Carrete, N. A. Katcho and N. Mingo, *Comput. Phys. Commun.*, 2014, **185**, 1747–1758.
35 A. N. Gandi and U. Schwingenschlögl, *Chem. Mater.*, 2014, **26**, 6628–6637.
36 J. Zhang, H. Liu, L. Cheng, J. Wei, J. Liang, D. Fan, J. Shi, X. Tang and Q. Zhang, *Sci. Rep.*, 2014, **4**, 6452.
37 A. Togo, F. Oba and I. Tanaka, *Phys. Rev. B: Condens. Matter*, 2008, **78**, 134106.
38 W. Li, L. Lindsay, D. A. Broido, D. A. Stewart and N. Mingo, *Phys. Rev. B: Condens. Matter*, 2012, **86**, 174307.
39 W. Li, N. Mingo, L. Lindsay, D. A. Broido, D. A. Stewart and N. A. Katcho, *Phys. Rev. B: Condens. Matter*, 2012, **85**, 195436.
40 X. Wang, A. M. Jones, K. L. Seyler, V. Tran, Y. Jia, H. Zhao, H. Wang, L. Yang, X. Xu and F. Xia, *Nat. Nanotechnol.*, 2015, **10**, 517–521.
41 S. Baroni, S. De Gironcoli, A. Dal Corso and P. Giannozzi, *Rev. Mod. Phys.*, 2001, **73**, 515.
42 H. Şahin, S. Cahangirov, M. Topsakal, E. Bekaroglu, E. Akturk, R. T. Senger and S. Ciraci, *Phys. Rev. B: Condens. Matter*, 2009, **80**, 155453.
43 S. Mishra, S. Satpathy and O. Jepsen, *J. Phys.: Condens. Matter*, 1997, **9**, 461.
44 H. Shi, D. Parker, M.-H. Du and D. J. Singh, *Phys. Rev. Appl.*, 2015, **3**, 014004.
45 K. Kuroki and R. Arita, *J. Phys. Soc. Jpn.*, 2007, **76**, 083707.
46 L. Yan-Li and Z. Dian-Na, *Commun. Theor. Phys.*, 2013, **60**, 233.
47 G. K. Madsen, *J. Am. Chem. Soc.*, 2006, **128**, 12140–12146.
48 T. M. Tritt, *Annu. Rev. Mater. Res.*, 2011, **41**, 433–448.
49 J. M. Ziman, J. M. Ziman and G. B. Physicist, *Electrons and phonons: the theory of transport phenomena in solids*, Clarendon Press, Oxford, UK, 2001.
50 X. Wei, Y. Wang, Y. Shen, G. Xie, H. Xiao, J. Zhong and G. Zhang, *Appl. Phys. Lett.*, 2014, **105**, 103902.
51 L. Lindsay, W. Li, J. Carrete, N. Mingo, D. Broido and T. Reinecke, *Phys. Rev. B: Condens. Matter*, 2014, **89**, 155426.
52 L. Zhu, G. Zhang and B. Li, *Phys. Rev. B: Condens. Matter*, 2014, **90**, 214302.
53 Y. Zhang, X. Ke, C. Chen, J. Yang and P. R. C. Kent, *Phys. Rev. B: Condens. Matter*, 2009, **80**, 024304.
54 D. Morelli, V. Jovovic and J. Heremans, *Phys. Rev. Lett.*, 2008, **101**, 035901.
55 G. J. Snyder and T. S. Ursell, *Phys. Rev. Lett.*, 2003, **91**, 148301.
56 S. R. Brown, S. M. Kauzlarich, F. Gascoin and G. J. Snyder, *Chem. Mater.*, 2006, **18**, 1873–1877.
57 E. S. Toberer, M. Christensen, B. B. Iversen and G. J. Snyder, *Phys. Rev. B: Condens. Matter*, 2008, **77**, 075203.
58 D. Kraemer and G. Chen, *Rev. Sci. Instrum.*, 2014, **85**, 045107.
59 K. S. Novoselov, A. K. Geim, S. Morozov, D. Jiang, Y. Zhang, S. a. Dubonos, I. Grigorieva and A. Firsov, *Science*, 2004, **306**, 666–669.
60 L. Tao, E. Cinquanta, D. Chiappe, C. Grazianetti, M. Fanciulli, M. Dubey, A. Molle and D. Akinwande, *Nat. Nanotechnol.*, 2015, **10**, 227–231.

Supplementary Information for

Thermoelectric Properties of Single-layer SnSe Sheet

Fancy Qian Wang, Shunhong Zhang, Jiabing Yu, and Qian Wang*

To get accurate lattice thermal conductivity κ_l, the convergence of three important parameters: cutoff radius (R_{cutoff}), scalebroad, and k-point grid density are examined carefully by using the ShengBTE code.[1] All interactions between atomic triplets at distances larger than R_{cutoff} can be discarded when the radius exceeds the range of physically relevant anharmonic interactions in the crystal. Considering both the symmetry of single-layer SnSe and calculation expense, R_{cutoff} is set as 6.5 Å (taking into account interactions up to the 21st coordination shell) to ensure the accuracy.

The convergence of κ_l with respect to k-points and scalebroad is well testified. We fixed k-points equal to 10×10×1, then κ_l gets convergence when scalebroad reaches 1.0; next scalebroad was fixed equal to 1.0, and we found κ_l converges when the k-point mesh grid reaches 30×30×1.

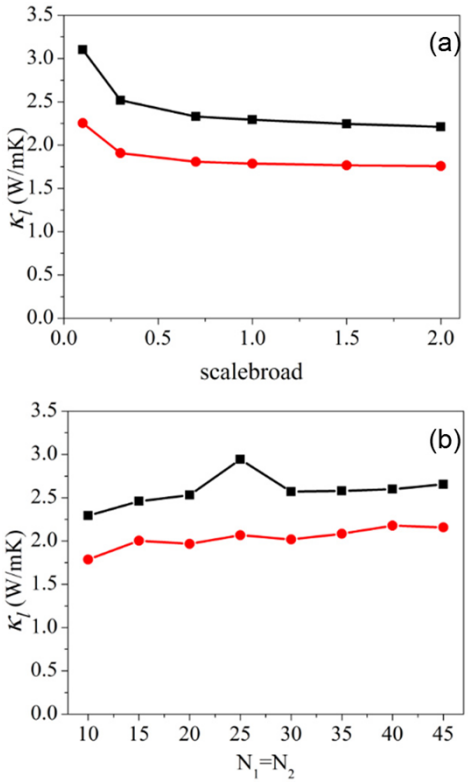

Fig. S1 Lattice thermal conductivity (κ_l) as a function of (a) scalebroad and (b) the grid density of k-points ($N_1 \times N_2 \times 1$) along the zigzag (black dots) and the armchair (red dots) direction.

To study the variance of the Sn-Se bond length with temperature, we classified the Sn-Se bonds into two types: namely the in plane Sn-Se bonds, labeled as d_1, and the Sn-Se bonds in the direction nearly perpendicular to the plane, labeled as d_2, as shown in Fig. S2. We have looked at the bond length variance carefully during the simulations at the different temperatures, and found that the bond lengths (d_1 and d_2) oscillate around their equilibrium bond lengths at 0 K. For comparison, the average bond lengths of d_1 and d_2 are summarized in Table S1, which shows that the change of average bond lengths $\bar{d}_1$ is less than 5% while that of $\bar{d}_2$ about 1%, as compared to their equilibrium bond lengths at 0 K, respectively.

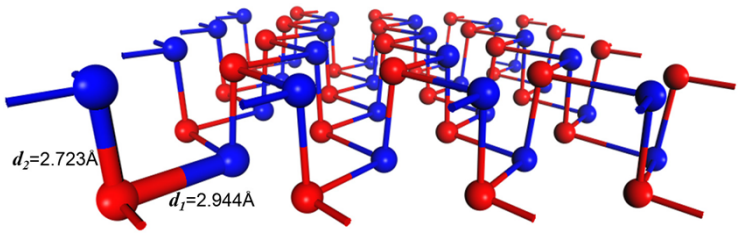

Fig. S2 Initial structure (0K) of single-layer SnSe from perspective view. Two types of bonds are bolded and labeled as d_1 and d_2. The typical bond length of d_1 and d_2 are 2.944Å and 2.723Å, respectively.

Table S1. The average bond length of single-layer SnSe at different temperatures (in Å)

	0 K	**300 K**	**500 K**	**700 K**	**900 K**
$\bar{d}_1$	2.944	2.981	3.004	3.087	3.116
$\bar{d}_2$	2.723	2.709	2.777	2.733	2.752

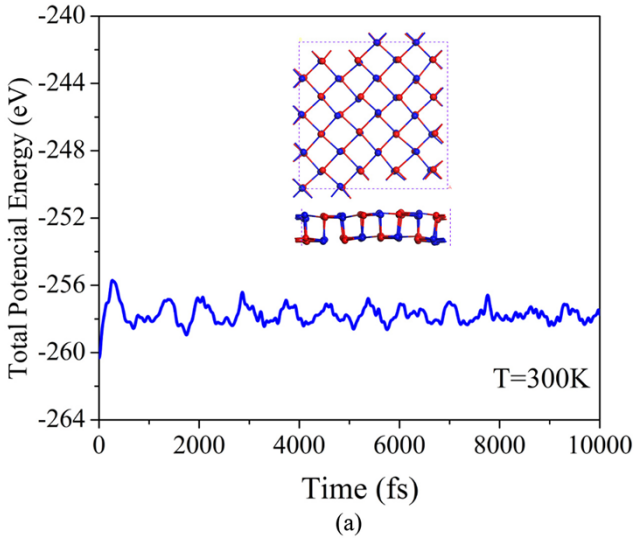

(a)

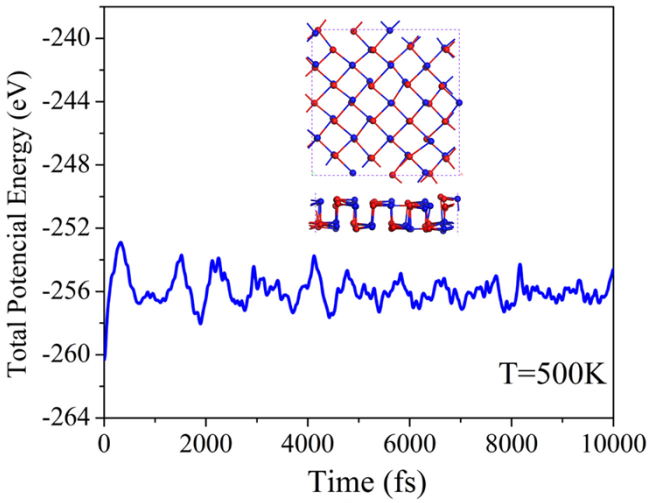
Total Potencial Energy (eV)
-240
-244
-248
-252
-256
-260
-264
0
2000
4000
6000
8000
10000
Time (fs)
T=500K

(b)

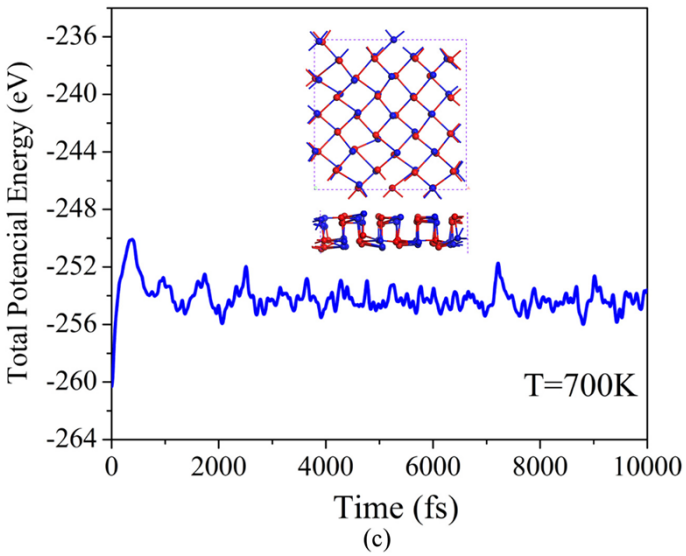
Total Potencial Energy (eV)
-236
-240
-244
-248
-252
-256
-260
-264
0
2000
4000
6000
8000
10000
Time (fs)
T=700K

(c)

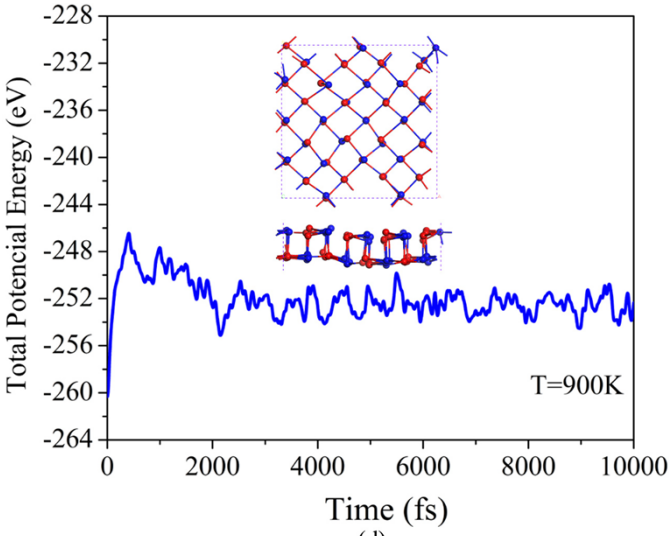
Total Potencial Energy (eV)
-228
-232
-236
-240
-244
-248
-252
-256
-260
-264
0
2000
4000
6000
8000
10000
Time (fs)
T=900K

(d)

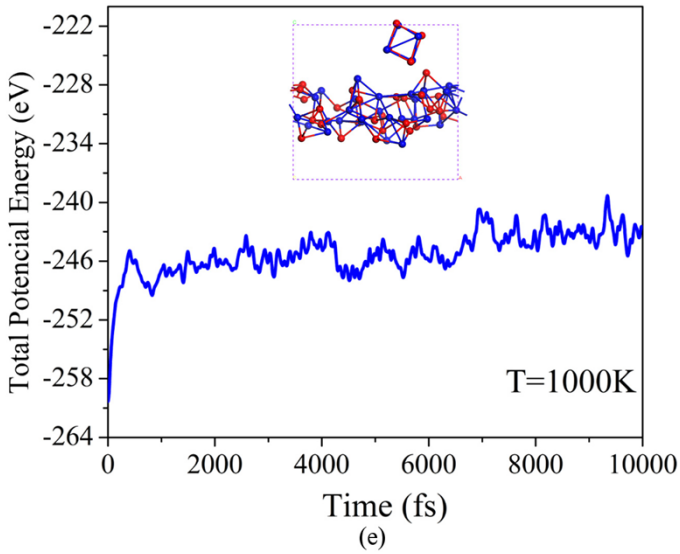

Fig. S3 Total potential energy fluctuation during AIMD simulation of single-layer SnSe at different temperatures, namely (a) 300 K, (b) 500K, (c) 700K, (d) 900K, and (e) 1000K. The insets show the snapshots of atomic configuration of single-layer SnSe at the end of AIMD simulation.

We calculated the thermal conductivity by solving the linearized phonon BTE with an iterative approach using ShengBTE code, which focuses on the anharmonic scattering and isotopic impurity scattering. In the isotopic impurity scattering process, higher frequency governs the thermal conductivity in the form of $A\omega^{-4}$, where A is a physical parameter depending on the nature of the point defects.[2] That means isotopic impurity scattering rates only has relationship with high frequency optical modes. In anharmonic phonon-phonon process we assume that only the acoustic phonon modes participate in the heat conduction process, the thermal conductivity can be expressed as $\kappa = B\frac{\overline{M}\theta_a^3\delta}{\gamma^2 n^{\frac{2}{3}}T}$,[3] where $\overline{M}$ is the average mass of an atom in the crystal (in atomic mass unit), θ_a is the Debye temperature of acoustic phonons, δ^3 is the volume per atom (δ in Å), n is the number of atoms in the

primitive unit cell, γ is the high temperature limit of the acoustic phonon mode Grüneisen parameter, and B≈3.1×10^{-6} is a collection of physical constants. When the anharmonic phonon-phonon interactions are dominant in phonon scattering mechanism, the lattice thermal conductivity is subject to the relationship $\kappa_l \propto \frac{1}{T}$. We fitted the κ_l-1/T curves using the least square fitting method. The curves exhibit perfect linearity is as shown in Fig. 5 (d), from where we obtain the scale factor to be 770.56 and 604.90 W/m for the zigzag and armchair directions, respectively.

The mode Grüneisen parameter is given as $\gamma_\lambda = -\frac{A}{\omega_\lambda}\frac{\partial\omega_\lambda}{\partial A}$, where A is the area of a unit cell of single-layer SnSe, and ω_λ is the angular frequency of a specific phonon mode. γ of the three acoustic modes is calculated using the Phonopy Package[4] and shown in Figure S4. To obtain reliable Grüneisen parameters, phonon calculations are performed in three individual lattices respectively, namely, the equilibrium lattice, as well as in the slightly stretched (+0.3%) and compressed lattice (-0.3%). The ZA mode diverges when its momentum approaches Γ point because of the quadratic band dispersion, similar to the cases in graphene and phosphorene.[5]

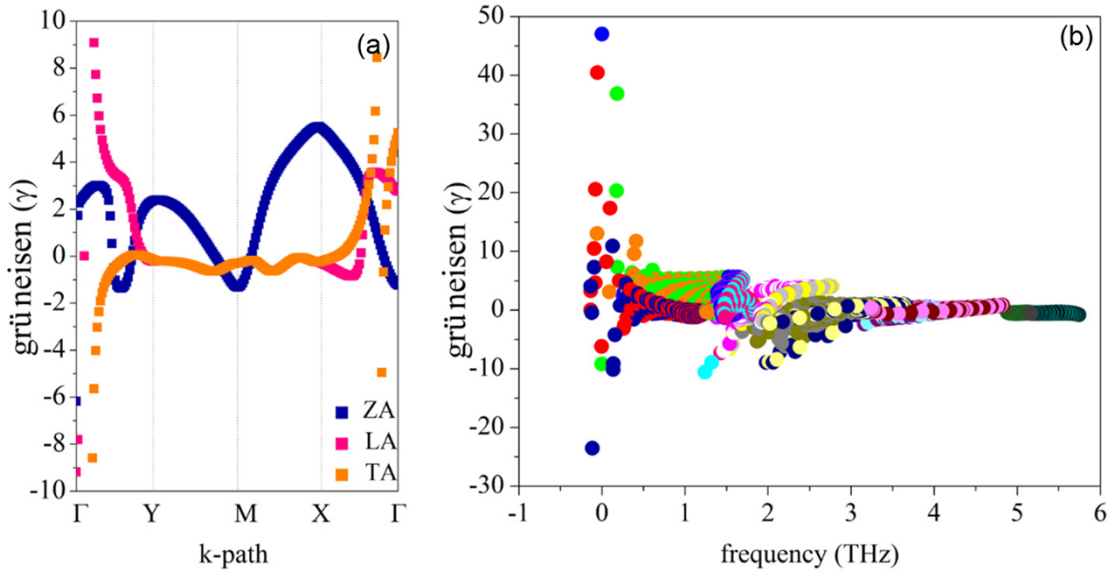

Fig. S4 Mode Grüneisen parameter (γ) of the acoustic modes of single-layer SnSe (a) along high symmetry point paths in the first Brillouin zone. (b) Frequency distribution of the mode Grüneisen parameter, calculated using a reciprocal mesh (31×31×1).

1. W. Li, J. Carrete, N. A. Katcho and N. Mingo, *Comput. Phys. Commun.*, 2014, **185**, 1747-1758.
2. P. Klemens, *Int. J. Thermophys.*, 2001, **22**, 265-275.
3. D. Morelli, V. Jovovic and J. Heremans, *Phys. Rev. Lett.*, 2008, **101**, 035901.
4. A. Togo, F. Oba and I. Tanaka, *Phys. Rev. B*, 2008, **78**, 134106.
5. R. Fei, A. Faghaninia, R. Soklaski, J.-A. Yan, C. Lo and L. Yang, *Nano. Lett.*, 2014, **14**, 6393-6399.